RESEARCH PAPER

Harnessing *Plectranthus vettiveroides* for Nanomedicine: Green synthesis of ZnO nanoparticles and their antioxidant and anticancer activities

Priyanka V.[1], H.R.Raveesha[1]*

[1]*Department of Botany, Jnanabharathi Campus,*
Bangalore University, Bengaluru – 560056, Karnataka, India
Corresponding Author:
Email ID : raveesha74@bub.ernet.in
Orcid ID: https://orcid.org/0000-0001-9860-1805

Received: 5th Jan, 2026; Revised: 25th Jan 2026; Accepted: 20th Feb, 2026; Available Online: 10th Mar, 2026

ABSTRACT
The present study explores the green synthesis of zinc oxide nanoparticles (ZnO NPs) using root extracts of *Plectranthus vettiveroides* (PVR) authentication number *(*RRCBI-mus660), a traditionally valued herb collected from Chidambaram, Tamil Nadu. Leveraging the phytochemical richness of the root matrix, ZnO NPs were synthesized via an eco-friendly protocol and characterized using UV-Vis spectroscopy, FTIR, XRD, SEM, and HR TEM to confirm their structural integrity, morphology, and crystalline nature. The biosynthesized ZnO nanoparticles from *Plectranthus vettiveroides* root extract exhibited a UV-Vis absorption peak shift indicating smaller particle size, with FTIR and XRD confirming functional groups and a hexagonal (wurtzite) crystalline structure. Morphological analysis revealed irregular, aggregated nanostructures (50–200 nm) with a negative zeta potential (−25.6 mV), affirming stability and polydispersity. PVR ZnO NPs exhibited highest antioxidant efficacy compared to ascorbic acid, with lower IC_{50} values and concentration-dependent activity confirmed via DPPH, ABTS, and FRAP assays, highlighting their potent redox-modulating capacity. Furthermore, the anticancer efficacy of the ZnO NPs was assessed against selected human cancer cell lines using MTT and morphological assays, demonstrating dose-dependent cytotoxicity and apoptotic features. The study underscores the dual bioactivity of ZnO NPs antioxidant and anticancer attributable to the synergistic interaction between zinc ions and bioactive phytoconstituents from *P. vettiveroides*. This work not only validates the therapeutic potential of a lesser-explored ethnomedicinal plant but also contributes to the growing field of phytogenic nanomedicine. The integration of green chemistry principles with biomedical applications offers a sustainable and translational approach for future cancer therapeutics. Further mechanistic studies and *in vivo* validations are warranted to elucidate the molecular pathways involved and to advance clinical relevance.

Keywords: Apoptosis, Cytotoxicity, Nanomedicine, *Plectranthus vettiveroides*, ZnO nanoparticles
How to cite this article: V P, H R. Harnessing *Plectranthus vettiveroides* for Nanomedicine: Green synthesis of ZnO nanoparticles and their antioxidant and anticancer activities. Int.. J Drug Deliv Technol. 2026;16(8s): 753-768; Doi: 10.25258/Ijddt.16.8s.84
Source of support: Nil.
Conflict of interest: None

INTRODUCTION

Nanotechnology has revolutionized biomedical sciences by enabling the development of functional nanomaterials with enhanced physicochemical and biological properties. Among metal oxide nanoparticles, zinc oxide (ZnO) has garnered significant attention due to its unique optical, catalytic, and therapeutic attributes. ZnO nanoparticles are biocompatible, exhibit a wide band gap (3.37 eV), and possess a high exciton binding energy (60 meV), making them suitable for applications ranging from drug delivery to cancer therapy and antioxidant modulation (Sukri *et al*., 2023).

Traditional chemical and physical methods for nanoparticle synthesis often involve toxic reagents, high energy input, and environmental hazards. In contrast, green synthesis using plant extracts offers a sustainable, cost-effective, and eco-friendly alternative. Phytochemicals such as flavonoids, terpenoids, alkaloids, and polyphenols act as reducing and stabilizing agents in nanoparticle formation, imparting bioactivity and structural stability (Golzarnezhad *et al*., 2025).

Green synthesis of ZnO nanoparticles using plant extracts has emerged as a viable alternative to conventional methods. Zheng *et al*. (2019) demonstrated the synthesis of ZnO NPs using *Plectranthus amboinicus* leaf extract, confirming their hexagonal wurtzite structure and enhanced electrochemical properties. Similarly, Chandrasekar *et al*. (2023) synthesized ZnO NPs from *P. amboinicus* for dye degradation and antibacterial activity, reporting strong Zn–O bonding and nanoflake morphology.

Oxidative stress plays a pivotal role in the pathogenesis of chronic diseases, including cancer, neurodegeneration, and

**Author for Correspondence: raveesha74@bub.ernet.in*

cardiovascular disorders. Antioxidants neutralize free radicals, thereby mitigating cellular damage. ZnO nanoparticles have demonstrated significant antioxidant activity due to their surface reactivity and ability to modulate redox pathways. Fatima *et al*. (2024) synthesized ZnO NPs using *Aerva persica* root extract and reported potent antioxidant activity comparable to ascorbic acid, validated through DPPH and FRAP assays. Momeni *et al*. (2023) showed that ZnO NPs synthesized from *Crataegus oxyacantha* leaf extract exhibited superior DPPH scavenging activity at 200 µg/mL compared to ascorbic acid.

Cancer remains a leading cause of mortality worldwide, necessitating novel therapeutic strategies with minimal side effects. ZnO nanoparticles have shown promise as anticancer agents due to their ability to induce reactive oxygen species (ROS), disrupt mitochondrial function, and trigger apoptosis in cancer cells. Perumal *et al*. (2024) synthesized ZnO NPs using Shilajit extract and reported cytotoxic effects against HeLa cells with an IC_{50} of 38.6 µg/mL, comparable to cisplatin. Golzarnezhad *et al*. (2025) demonstrated that ZnO NPs from *Cymbopogon olivieri* extract significantly reduced ovarian cancer cell viability, with an IC_{50} of 350 µg/mL.

Plectranthus vettiveroides, a lesser-explored ethnomedicinal herb endemic to southern India, belongs to the Lamiaceae family and is traditionally used for its anti-inflammatory, antimicrobial, and wound-healing properties. Its root extract is rich in bioactive compounds, making it a promising candidate for nanoparticle synthesis. This study aims to synthesize ZnO nanoparticles using *P. vettiveroides* root extract, characterize their physicochemical properties, and evaluate their antioxidant and anticancer potential.

MATERIAL AND METHODS

Collection and Preparation of Plant Material

Fresh roots of *Plectranthus vettiveroides* were collected from Chidambaram, Tamil Nadu, India, during the early monsoon season to ensure optimal phytochemical content. The plant specimen was authenticated by Central ayurveda research centre, Bengaluru and authenticated number - *(*RRCBI-mus660). Roots were thoroughly washed with distilled water to remove soil and debris, shade-dried for 7–10 days, and ground into fine powder using a mechanical grinder. 10 g of powdered root was boiled in 100 mL of distilled water at 60–70°C for 30 minutes. The extract was filtered using Whatman No. 1 filter paper and stored at 4°C for further use.

Green Synthesis of ZnO Nanoparticles

Zinc acetate dihydrate [$Zn(CH_3COO)_2 \cdot 2H_2O$] was used as the zinc source. 50 mL of *P. vettiveroides* root extract was added dropwise to 100 mL of 0.01 M zinc acetate solution under constant stirring at 60°C. The pH was adjusted to 10 using 1 M NaOH to facilitate precipitation. The reaction mixture was stirred for 3 hours until a pale white precipitate formed. The precipitate was centrifuged at 10,000 rpm for 15 minutes, washed thrice with distilled water and ethanol, and dried at 80°C overnight. The dried powder was calcined at 400°C for 2 hours to obtain ZnO nanoparticles (Ala Nissila *et al*., 2012).

Characterization of PVR ZnO Nanoparticles

UV-Visible Spectroscopy

Absorption spectra were recorded using a UV-Vis spectrophotometer (200–800 nm). A peak shift toward shorter wavelengths indicated smaller particle size.
P. vettiveroides extract showed a peak at 275 nm.

Fourier Transform Infrared Spectroscopy (FTIR)

Fourier Transform Infrared (FTIR) spectroscopy was employed to identify the functional groups involved in the reduction and stabilization of ZnO nanoparticles synthesized from *P. vettiveroides* root extract. The dried ZnO nanoparticles sample was finely ground and mixed with potassium bromide (KBr) in a 1:100 ratio to form a translucent pellet using a hydraulic press. The pellet was then analyzed using an FTIR spectrophotometer in the spectral range of 4000–400 cm^{-1}. The resulting spectra revealed characteristic peaks corresponding to various phytochemical constituents and metal-oxygen interactions.

X-ray Diffraction (XRD)

XRD analysis was performed to determine the crystalline structure, phase purity, and average crystallite size of the ZnO nanoparticles synthesized using *P. vettiveroides* root extract. The dried nanoparticles powder was mounted on a sample holder and scanned using an X-ray diffractometer equipped with Cu-Kα radiation ($\lambda = 1.5406$ Å), operating at 40 kV and 30 mA. The diffraction patterns were recorded over a 2θ range of 10° to 80° at a scanning rate of 2° per minute.

Energy Dispersive X-ray Analysis (EDAX)

EDAX was employed to determine the elemental composition and purity of the ZnO nanoparticles synthesized from *P. vettiveroides* root extract. The dried nanoparticle sample was mounted onto a carbon-coated stub and subjected to scanning under a field emission scanning electron microscope (FESEM) equipped with an EDAX detector. The analysis was conducted at an accelerating voltage of 15–20 kV to ensure optimal excitation of characteristic X-rays.

Scanning Electron Microscopy (SEM) and High resolution - Transmission Electron Microscopy (HR TEM)

SEM and HR TEM were employed to investigate the surface morphology, particle size, and structural features of the zinc oxide nanoparticles synthesized from *P. vettiveroides* root extract. For SEM analysis, a thin layer of the dried nanoparticle powder was mounted on a carbon-coated stub and sputter-coated with gold to enhance conductivity. The sample was visualized under a field emission SEM operated at an accelerating voltage of 15–20 kV. SEM images revealed irregularly shaped, aggregated nanostructures with porous and rough surface textures, typical of biosynthesized metal oxides. For TEM analysis, a small amount of ZnO nanoparticle suspension was

dropped onto a carbon-coated copper grid and allowed to dry under ambient conditions.

Zeta Potential Analysis

Zeta potential analysis was conducted to evaluate the surface charge and colloidal stability of the ZnO nanoparticles synthesized from *P. vettiveroides* root extract. Aqueous suspensions of the dried ZnO nanoparticles were prepared by dispersing 1 mg/mL of the sample in deionized water, followed by ultrasonication for 15 minutes to ensure uniform dispersion. The measurements were performed using a dynamic light scattering (DLS) instrument equipped with a zeta potential analyzer, operating at room temperature. The electrophoretic mobility of the nanoparticles was recorded and converted to zeta potential values using the Smoluchowski equation.

Photocatalytic Activity

The photocatalytic activity of the biosynthesized ZnO nanoparticles from *P. vettiveroides* root extract was evaluated using the degradation of methylene blue (MB) dye as a model pollutant under UV irradiation. Aqueous suspensions of ZnO NPs (1 mg/mL) were prepared and sonicated for 10 minutes to ensure uniform dispersion. In a typical experiment, 50 mL of 10 ppm methylene blue solution was mixed with 10 mg of ZnO NPs and stirred in the dark for 30 minutes to establish adsorption–desorption equilibrium. The mixture was then exposed to UV light (λ = 365 nm) using a UV chamber equipped with a mercury vapor lamp. Aliquots were withdrawn at regular intervals (0, 15, 30, 45, 60, and 90 minutes), centrifuged to remove nanoparticles, and the absorbance of the supernatant was measured at 664 nm using a UV-Vis spectrophotometer (Asif *et al*., 2025; Pandey *et al*., 2013). The percentage degradation of methylene blue was calculated using the formula:

Degradation (%) = $[(A_0 - A_t)/A_0] \times 100$,

where A_0 is the initial absorbance and A_t is the absorbance at time *t*. The photocatalytic efficiency was assessed based on the rate of dye degradation, and the results indicated a time-dependent decrease in absorbance, confirming the photocatalytic potential of the ZnO NPs. The enhanced activity is attributed to the nanoscale size, surface roughness, and crystalline nature of the particles, which facilitate effective generation of reactive oxygen species under UV exposure.

Biological Studies of ZnO NPs of *P. vettiveroides* root extract

Antioxidants Activities

DPPH FREE RADICAL POTENTIAL ASSAY

The antioxidant activity of the biosynthesized ZnO NPs from *P. vettiveroides* root extract was evaluated using the DPPH radical scavenging assay, a widely accepted method for assessing free radical neutralization potential. A stock solution of 0.1 mM DPPH was prepared in methanol and stored in the dark to prevent photodegradation. Various concentrations of ZnO NPs (ranging from 1 to 100 µg/mL) were mixed with 2 mL of the DPPH solution and incubated at room temperature for 30 minutes in the absence of light. The reduction in absorbance was measured at 517 nm using a UV-Visible spectrophotometer. Ascorbic acid was used as the standard antioxidant for comparison (Shah *et al*., 2015; Chaves *et al*., 2020).

The percentage of radical scavenging activity was calculated using the formula:

% Inhibition = $[(A_0 - A_1)/A_0] \times 100$

where A_0 is the absorbance of the control (DPPH alone) and A_1 is the absorbance of the sample. The IC_{50} value, representing the concentration required to inhibit 50% of the DPPH radicals, was determined from the dose–response curve.

ABTS ASSAY

The ABTS radical cation decolorization assay was employed to evaluate the antioxidant potential of ZnO NPs synthesized from *P. vettiveroides* root extract. The $ABTS^{\bullet+}$ radical was generated by reacting 7 mM ABTS solution with 2.45 mM potassium persulfate and incubating the mixture in the dark at room temperature for 12–16 hours. The resulting blue-green $ABTS^{\bullet+}$ solution was diluted with methanol to obtain an absorbance of 0.70 ± 0.02 at 734 nm. Various concentrations of ZnO NPs (1–100 µg/mL) were added to 2 mL of the $ABTS^{\bullet+}$ working solution and incubated for 30 minutes in the dark. The reduction in absorbance was measured at 734 nm using a UV-Visible spectrophotometer. Ascorbic acid was used as the standard antioxidant for comparison (Shah *et al*., 2015; Chaves *et al*., 2020).

The percentage inhibition of ABTS radicals was calculated using the formula:

% Inhibition = $[(A_0 - A_1)/A_0] \times 100$

where A_0 is the absorbance of the control and A_1 is the absorbance of the sample. The IC_{50} value was determined from the dose–response curve.

FRAP ASSAY

The Ferric Reducing Antioxidant Power (FRAP) assay was conducted to assess the electron-donating capacity of ZnO NPs synthesized from root extract. The assay is based on the reduction of ferric (Fe^{3+}) to ferrous (Fe^{2+}) ions in the presence of antioxidants, forming a blue-colored ferrous–tripyridyltriazine complex that can be quantified spectrophotometrically. The FRAP reagent was freshly prepared by mixing 300 mM acetate buffer (pH 3.6), 10 mM TPTZ (2,4,6-tripyridyl-s-triazine) in 40 mM HCl, and 20 mM $FeCl_3 \cdot 6H_2O$ in a 10:1:1 ratio. ZnO NPs samples at various concentrations (1–100 µg/mL) were added to 2 mL of FRAP reagent and incubated at 37°C for 30 minutes. The absorbance was measured at 593 nm using a UV-Visible spectrophotometer. Ascorbic acid was used as the standard reference compound. The antioxidant capacity was expressed in terms of ascorbic acid equivalents (AAE), and

a concentration-dependent increase in reducing power was observed across all tested samples (Shah *et al*., 2015; Chaves *et al*., 2020).

Anticancer Activity

Cell viability tests: MTT assay

The cytotoxic potential of the biosynthesized ZnO NPs from *P. vettiveroides* root extract was assessed using the MTT[3-(4,5-dimethylthiazol-2-yl)-2,5diphenyltetrazolium bromide] assay, the cytotoxicity effect of PVR was analyzed on A549, HCT-116 and MCF7 cells by performing the MTT assay (Ghasemi *et al*., 2021). MTT is a tetrazolium salt which is converted into insoluble purple-colored formazan crystals by the action of lactate dehydrogenase enzyme released by mitochondria. Briefly, cells in 200µL of suitable media and at a density of 10,000 were plated in a 96-well plate and incubated at 37 °C for overnight. After attachment of cells to the surface of cell culture plate, the spent medium was replaced with complete media having various working concentrations of ZnO NPs PVR (12.5, 25, 50, 100 and 200µg/mL). After drug addition, cells were incubated for 24hrs at 37 °C with 5% CO_2 atmosphere. After incubation, cells were treated with 100µL of MTT (0.5 mg/mL) was added and incubated for 3hrs at 37 °C. DMSO (100µL) was used to dissolve the formazan crystals, and purple color was measured at 570 nm using microplate reader (ELX-800, BioTek, USA). The viability of cells treated with DMEM alone was considered as 100%. % cell viability is calculated using the below formula:

% cell viability = [OD of treated cells/OD of Untreated cells] x 100

The IC_{50} value was determined by using linear regression equation i.e. Y =Mx+C. Here, Y = 50, M and C values were derived from the viability graph.

Apoptosis/Necrosis study by Flow Cytometry in ZnO NPs PVR Annexin V/PI staining in MCF-7 cells by FACS Analysis

To evaluate the apoptotic and necrotic effects of ZnO NPs synthesized from *P. vettiveroides* root extract, Annexin V-FITC/Propidium Iodide (PI) dual staining was performed on human breast cancer MCF-7 cells, followed by analysis using flow cytometry (FACS). MCF-7 cells were cultured in DMEM supplemented with 10% fetal bovine serum and 1% penicillin-streptomycin, maintained at 37°C in a humidified 5% CO_2 incubator. Cells were seeded in 6-well plates at a density of 2×10^5 cells/well and treated with ZnO NPs PVR at selected concentrations for 24 hrs. Post-treatment, cells were harvested by trypsinization, washed twice with cold phosphate-buffered saline (PBS), and resuspended in 100 µL of binding buffer. Annexin V-FITC (5 µL) and PI (5 µL) were added to each sample and incubated in the dark at room temperature for 15 minutes. After incubation, 400 µL of binding buffer was added, and samples were immediately analyzed using a flow cytometer equipped with appropriate filters for FITC and PI detection. Data were acquired for 10,000 events per sample and analyzed using quadrant gating to distinguish viable cells (Annexin V^-/PI^-), early apoptotic cells (Annexin V^+/PI^-), late apoptotic cells (Annexin V^+/PI^+), and necrotic cells (Annexin V^-/PI^+). The results revealed a dose-dependent increase in apoptotic populations, confirming the cytotoxic and pro-apoptotic potential of the biosynthesized ZnO NPs PVR against MCF-7 cells (Fox and Aubert, 2008).

Cell cycle analysis by Flow Cytometry in ZnO NPs PVR in FACS: PI/RNAse Staining

Cell cycle distribution of MCF-7 cells treated with ZnO NPs synthesized from *P. vettiveroides* root extract was analyzed using flow cytometry following PI/RNase staining. MCF-7 cells were cultured in DMEM supplemented with 10% fetal bovine serum and 1% penicillin-streptomycin, maintained at 37°C in a humidified incubator with 5% CO_2. Cells were seeded in 6-well plates at a density of 2×10^5 cells/well and treated with ZnO NPs PVR at selected concentrations for 24 hrs. Post-treatment, cells were harvested by trypsinization, washed twice with cold phosphate-buffered saline (PBS), and fixed in 70% chilled ethanol overnight at −20°C to preserve nuclear integrity. Fixed cells were washed with PBS and incubated with staining solution containing 50 µg/mL propidium iodide and 100 µg/mL RNase A in PBS for 30 minutes at 37°C in the dark. Flow cytometric analysis was performed using a FACS system equipped with a 488 nm laser, and data were acquired for 10,000 events per sample. PI fluorescence was measured in the FL2 channel, and cell cycle phases (G_0/G_1, S, and G_2/M) were quantified using appropriate software by gating based on DNA content histograms. The results revealed alterations in cell cycle progression, including accumulation of cells in sub-G_1 and G_2/M phases, indicative of nanoparticle-induced cell cycle arrest and apoptotic DNA fragmentation.

Measurement of ROS expression by Flow Cytometry in ZnO NPs PVR induced MCF7 cells by FACS Analysis

To assess intracellular reactive oxygen species (ROS) generation in MCF-7 cells following treatment with ZnO NPs, a flow cytometry-based assay using the fluorescent probe 2′,7′-dichlorodihydrofluorescein diacetate (DCFH-DA) was performed. MCF-7 cells were cultured in DMEM supplemented with 10% fetal bovine serum and 1% penicillin-streptomycin, maintained at 37°C in a humidified 5% CO_2 incubator. Cells were seeded in 6-well plates at a density of 2×10^5 cells/well and treated with PVR-ZnO NPs at selected concentrations for 24 hrs. Post-treatment, cells were harvested by trypsinization, washed twice with cold phosphate-buffered saline (PBS), and incubated with 10 µM DCFH-DA in serum-free medium for 30 minutes at 37°C in the dark. The non-fluorescent DCFH-DA diffuses into cells and is hydrolyzed by intracellular esterases to DCFH, which is then oxidized by ROS to form the highly fluorescent compound DCF. After incubation, cells were washed, resuspended in PBS, and immediately analyzed using a flow cytometer equipped with a 488 nm excitation laser and a 530 nm emission filter (FL1 channel). A total of 10,000 events per sample were recorded, and mean fluorescence intensity (MFI) was quantified to determine

ROS levels. The results demonstrated a dose-dependent increase in ROS expression in PVR ZnO NPs treated cells compared to untreated controls, indicating oxidative stress induction and supporting the pro-apoptotic mechanism of the nanoparticles.

Measurement of Caspase-3 expression by Flow Cytometry in PVR ZnO NPs induced MCF7 cells by FACS Analysis

To investigate the apoptotic mechanism induced by ZnO NPs synthesized from *P. vettiveroides* root extract, Caspase-3 expression was quantified in MCF-7 cells using flow cytometry. MCF-7 cells were cultured in DMEM supplemented with 10% fetal bovine serum and 1% penicillin-streptomycin, maintained at 37°C in a humidified atmosphere with 5% CO_2. Cells were seeded in 6-well plates at a density of 2×10^5 cells/well and treated with PVR-ZnO NPs at selected concentrations for 24 hrs. Following treatment, cells were harvested by trypsinization, washed twice with cold phosphate-buffered saline (PBS), and fixed in 4% paraformaldehyde for 15 minutes at room temperature. After fixation, cells were permeabilized using 0.1% Triton X-100 in PBS for 10 minutes and incubated with fluorochrome-conjugated anti-Caspase-3 antibody (e.g., FITC or PE-labelled) for 30 minutes in the dark. Unbound antibodies were removed by washing with PBS, and cells were resuspended in 500 µL of PBS for analysis. Flow cytometry was performed using a FACS system equipped with appropriate filters for the selected fluorochrome, and data were acquired for 10,000 events per sample. The mean fluorescence intensity (MFI) and percentage of Caspase-3–positive cells were quantified using flow cytometry software. A dose-dependent increase in Caspase-3 expression was observed in PVR ZnO NPs treated cells compared to untreated controls, confirming activation of the intrinsic apoptotic pathway (Srivastava *et al*., 2022).

RESULTS

UV-Visible Spectroscopy of PVR ZnO NPs

Absorption spectra were recorded using a UV-Vis spectrophotometer (200–800 nm). A peak shift toward shorter wavelengths indicated smaller particle size and observed PVR ZnO NPs showed a peak at 275 nm.

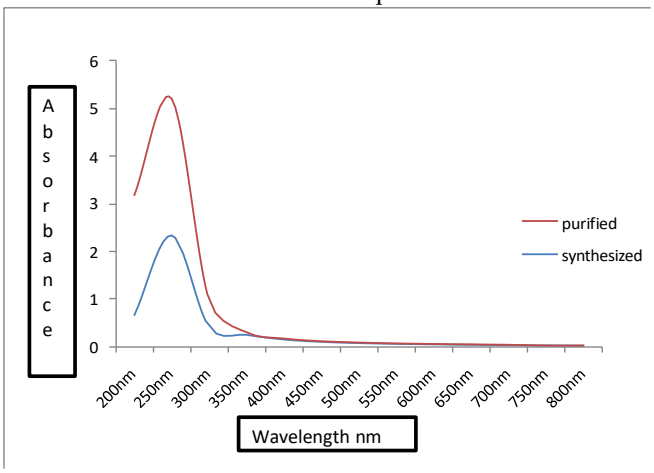

Figure 1: UV-Vis spectra show a peak at 275 nm for *P. vettiveroides* root extract, while ZnO nanoparticles exhibit a blue shift in absorption, indicating reduced particle size due to successful green synthesis.

Fourier Transform Infrared Spectroscopy (FTIR) of PVR ZnO NPs

The FTIR spectrum of ZnO NPs revealed distinct absorption bands indicative of phytochemical-mediated stabilization and successful nanoparticle formation. A broad peak at 3365 cm^{-1} corresponds to O–H stretching vibrations of polymeric hydroxyl groups, suggesting the presence of polyphenolic compounds from the extract acting as capping agents. Characteristic alkene (C=C) stretching was observed at 1624 cm^{-1} and 876 cm^{-1}, confirming the involvement of unsaturated phytoconstituents in nanoparticles synthesis. Prominent peaks at 663, 637, and 606 cm^{-1} were attributed to C–Br stretching, while bands at 566 and 540 cm^{-1} indicated C–I stretching, both representing halo compounds likely derived from secondary metabolites. Crucially, Zn–O stretching vibrations were detected at 762 and 588 cm^{-1}, validating the formation of zinc oxide nanoparticles. Absence of peaks corresponding to amine salts, alkanes, carboxylic acids, aliphatic amines, and secondary alcohols suggests selective phytochemical interaction during nanoparticle formation. These spectral features collectively confirm the role of *P. vettiveroides* root extract in reducing, stabilizing, and functionalizing ZnO nanoparticles through specific bioactive moieties.

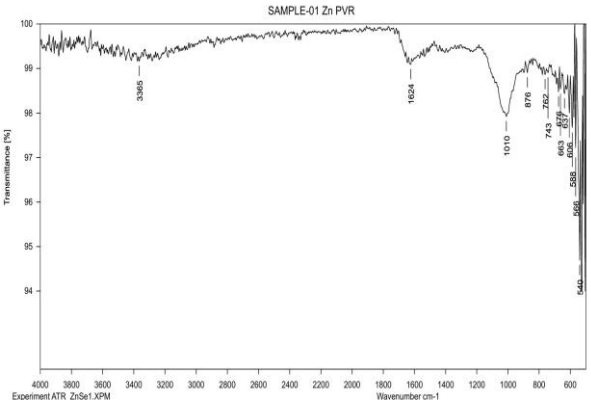

Figure 2: FTIR spectrum of PVR ZnO NPs nanoparticles shows key functional groups including O–H, C=C, C–Br, C–I, and Zn–O stretches, confirming phytochemical capping and successful nanoparticle formation.

X-ray Diffraction (XRD) of PVR ZnO NPs

ZnO NPs *Plectranthus vettiveroides* root, the highest characteristic peak was at 2θ value of 39.2 at the (1 0 1) crystallographic plane. The smaller peaks correspond to the noise and the other impurities, as the nanoparticles were prepared from plant extract.

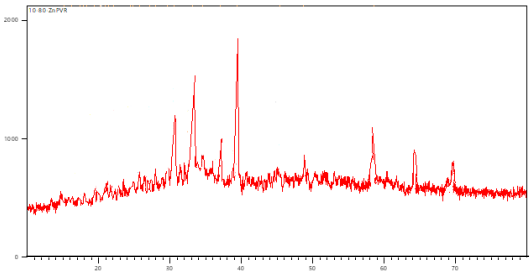

Scanning Electron Microscopy SEM EDAX of PVR ZnO NPs

SEM revealed that the PVR ZnO NPs exhibit aggregated nanostructures with porous and rough-surfaced morphology. The particles appeared irregularly shaped and grainy, which is characteristic of biosynthesized metal oxides. The nanoparticle clusters ranged from approximately 50 to 150 nm in diameter, indicating polydispersity and surface heterogeneity likely influenced by phytochemical capping agents. Energy Dispersive X-ray Analysis (EDAX) further confirmed the elemental composition of the sample, showing predominant peaks for zinc (Zn) and oxygen (O), consistent with the formation of ZnO nanoparticles. Quantitative analysis revealed a weight percentage of 47.52% for Zn and 42.48% for O, with corresponding atomic percentages of 48.40% and 31.60%, respectively. These results validate the successful green synthesis of ZnO NPs and support their purity and structural integrity. The EDAX spectrum, with the elemental composition box positioned in the top right corner, visually reinforces the ZnO identity of the sample.

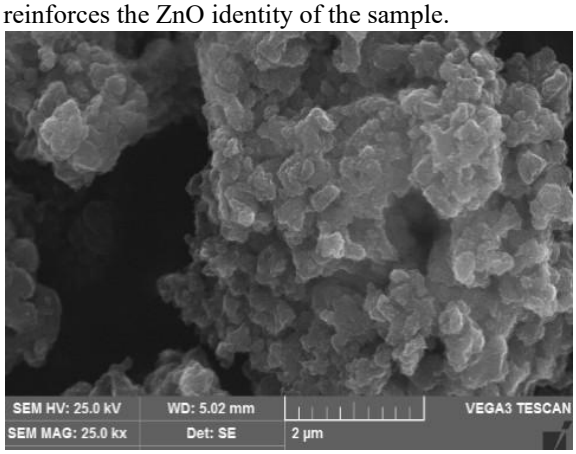

Figure 3: SEM micrograph of PVR ZnO nanoparticles reveals irregular, aggregated nanostructures with porous and rough surfaces, typical of biosynthesized metal oxides, ranging from 50 to 150 nm in diameter.

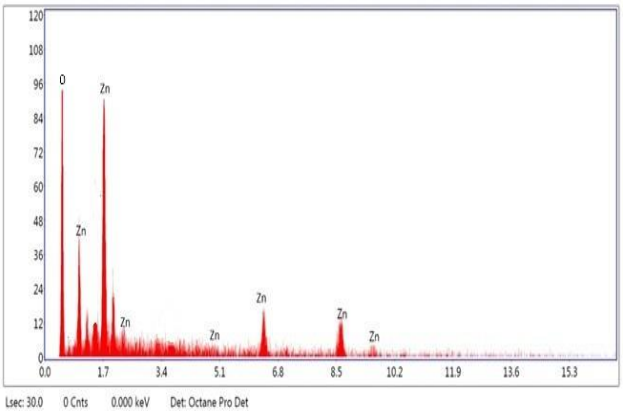

Figure 4: EDAX spectrum of PVR ZnO nanoparticles confirms elemental composition with dominant peaks for zinc (47.52% wt) and oxygen (42.48% wt), validating the purity and formation of zinc oxide nanoparticles.

HR TEM Analysis of PVR ZnO NPs

The HR TEM micrographs of PVR ZnO nanoparticles provide critical insights into their morphology, aggregation behaviour, and crystallinity across multiple magnification scales. At 100 nm magnification (Fig. 1-g), the nanoparticles appear as densely packed clusters ranging from 170–200 nm in diameter. This aggregation suggests strong interparticle interactions, likely mediated by phytochemical constituents from the root extract acting as natural stabilizers and bridging agents. The clustering also reflects the biosynthetic nature of the process, where uniform dispersion is often challenged by the complexity of plant-derived capping molecules.

At 50 nm magnification (Fig. 1-h), the surface texture of the nanoparticles becomes more discernible, revealing a rough and uneven topology. This morphological heterogeneity implies polydispersity in particle size and shape, a common feature in green-synthesized nanomaterials. The rough surfaces may enhance biological interactions, particularly in cellular uptake and reactive oxygen species (ROS) generation, contributing to the observed antioxidant and anticancer activities.

Further magnification at 20 nm (Fig. 1-i) shows nanoparticles that are embedded and sintered together, with regions of mixed contrast. This variation in contrast indicates uneven electron density, which may be attributed to differences in particle thickness, internal voids, or compositional heterogeneity. The sintering effect suggests partial fusion of particles during calcination, which can influence surface area and reactivity.

At the highest magnification of 5 nm (Fig. 1-j), the nanoparticles exhibit a fine granular structure without distinct lattice fringes. The absence of well-defined fringes points to low crystallinity at the nanoscale, although the overall diffraction data confirmed a hexagonal wurtzite structure. This discrepancy may arise from surface amorphization or the presence of organic residues from the plant extract, which obscure lattice visibility under high-resolution imaging.

Collectively, the HR TEM analysis confirms that PVR ZnO nanoparticles are irregular, polydisperse, and aggregated

with multiple crystalline domains. The structural features ranging from rough surfaces to low crystallinity are consistent with biosynthetic ZnO nanoparticles and may contribute to their enhanced biological performance. The confirmation of hexagonal wurtzite phase aligns with XRD findings, reinforcing the structural integrity of the synthesized nanomaterial.

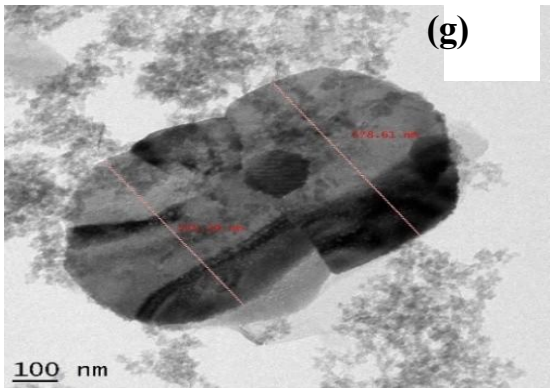

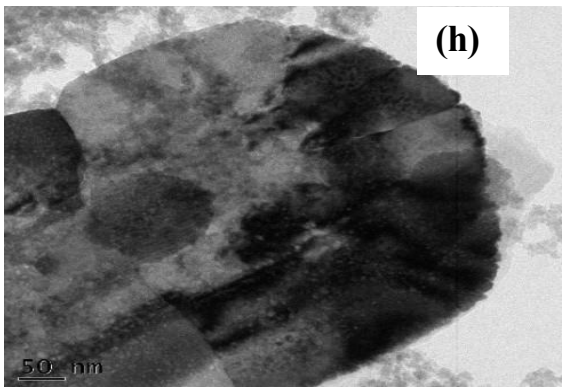

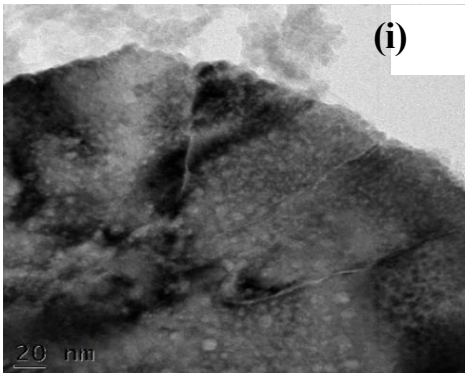

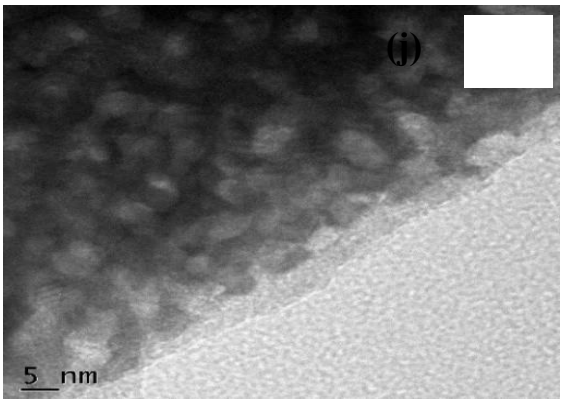

Figure 5: The HR TEM images of PVR ZnO NPs shows irregular and aggregated particles with multiple crystalline domains. The 100 nm magnification **(Fig. 1-g)** indicates the particle clusters, ranging from 170-200 nm, suggesting aggregated or dense particles. With higher magnification at 50 nm **(Fig. 1-h)**, rough surface texture is revealed, implying polydispersity. At 20 nm **(Fig. 1-i)**, the nanoparticles are more embedded and mostly sintered together, and the presence of mixed contrast indicates uneven density and size variation. The highest magnification scale at 5 nm **(Fig. 1-j)** shows fine granular structure without clear lattice fringes which suggests low crystallinity. Overall, the hexagonal crystal structure was confirmed, suggesting wurzite.

Zeta Potential and Particle analyser of PVR ZnO NPs

The particle size and surface charge characteristics of PVR ZnO NPs were evaluated using dynamic light scattering (DLS) and zeta potential analysis. The DLS-based particle size distribution revealed that 50% of the nanoparticles (D_{50} value) measured approximately 92.6 nm in diameter, indicating a nanoscale range suitable for biomedical applications. The distribution curve showed moderate polydispersity, consistent with the biosynthetic nature of the nanoparticles, where phytochemical variability influences nucleation and growth kinetics. The observed size range aligns with SEM and HR TEM findings, which also confirmed the presence of aggregated and irregularly shaped nanostructures.

Zeta potential analysis was performed to assess the colloidal stability and surface charge of the nanoparticle suspension. The PVR ZnO nanoparticles exhibited a zeta potential of −25.6 mV, indicating a moderately stable dispersion with negative surface polarity. This negative charge is attributed to the presence of anionic phytochemicals - such as hydroxyl and carboxyl groups originating from the *P. vettiveroides* root extract, which act as natural capping agents. The electrostatic repulsion between particles helps prevent aggregation, thereby enhancing suspension stability and biological compatibility. A zeta potential value beyond ±25 mV is generally considered sufficient to maintain colloidal stability, suggesting that the synthesized nanoparticles are suitable for further *in vitro* and *in vivo* applications, including antioxidant and anticancer evaluations.

Zeta Potential	
Mobility	-0.01u/ s/ V/ cm
Zeta Potential	-25.6 mv
Charge	-0.00009 fC
Polarity	Negative
Conductivity	1,571 uS/ cm
Field Strength	3.7 kV/ m
Sample Information	
Fluid	
ZN PVR	
Viscosity	0.81
Temperature	29.26 C
Dielectric Const	79
Dispersant	
pH	7

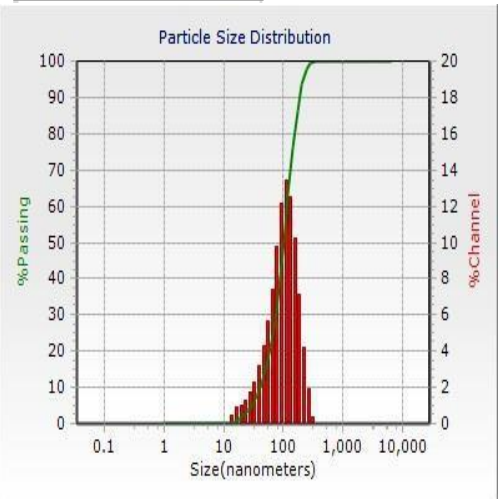

Figure 6: Particle size analysis and Zeta potential of of PVR ZnO NPs

Photocatalytic Activity of PVR ZnO NPs

The photocatalytic efficiency of ZnO NPs synthesized from *P. vettiveroides* root extract was evaluated through the degradation of methylene blue dye under UV irradiation over a time course of 180 minutes. At the initial time point (0 minutes), a baseline degradation of 14.51% was observed, likely due to adsorption of dye molecules onto the nanoparticle surface. Upon exposure to UV light, the degradation efficiency increased progressively, reaching 20.53% at 30 minutes and 27.83% at 60 minutes, indicating the onset of photocatalytic activity. A marked acceleration was noted at 90 minutes, with 42.15% degradation, followed by 50.06% at 120 minutes and 56.52% at 150 minutes. The maximum degradation recorded was 59.56% at 180 minutes, demonstrating sustained photocatalytic performance.

The time-dependent increase in dye degradation confirms the ability of PVR ZnO nanoparticles to generate reactive oxygen species (ROS) under UV light, facilitating oxidative breakdown of the dye molecules. The porous, rough-surfaced morphology and moderate particle size (50–150 nm) observed in SEM and HR TEM analyses likely contributed to enhanced surface area and light absorption, thereby improving photocatalytic efficiency. These findings underscore the potential of biosynthesized ZnO nanoparticles as eco-friendly photocatalysts for environmental remediation applications.

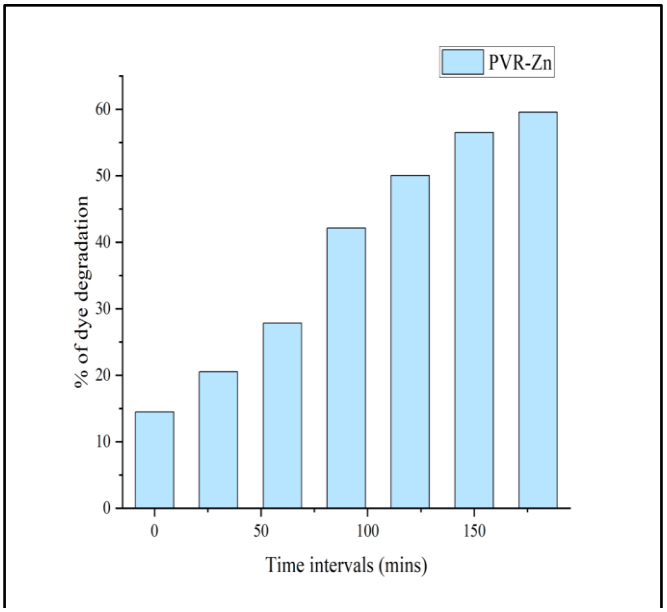

Figure 7: Photocatalytic Activity of PVR ZnO NPs showing dye degradation

Biological Studies of PVR ZnO NPs

DPPH Activity

The antioxidant potential of PVR ZnO NPs was assessed using the DPPH (2,2-diphenyl-1-picrylhydrazyl) radical scavenging assay, with ascorbic acid serving as the standard reference. The assay demonstrated a concentration-dependent increase in free radical scavenging activity for both PVR ZnO NPs and ascorbic acid across the tested range of 3.125 to 100 µg/mL. Notably, PVR ZnO NPs exhibited superior activity at lower concentrations, with 38.76 ± 2.4% inhibition at 3.125 µg/mL compared to 23.04 ± 2.1% for ascorbic acid. At 6.25 µg/mL, both samples showed comparable activity, while at 12.5 µg/mL and above, PVR ZnO NPs consistently outperformed the standard, reaching a maximum inhibition of 99.20 ± 1.5% at 100 µg/mL.

The IC_{50} value for PVR ZnO NPs was calculated as 3.95 ± 0.199 µg/mL, which is significantly lower than that of ascorbic acid (5.01 ± 0.235 µg/mL), indicating higher antioxidant efficacy. This enhanced activity is attributed to the synergistic interaction between zinc ions and phytochemical constituents from the *P. vettiveroides* root extract, which likely contribute to electron donation and radical neutralization. The results affirm the potent redox-modulating capacity of the biosynthesized nanoparticles and support their application in oxidative stress related therapeutic interventions.

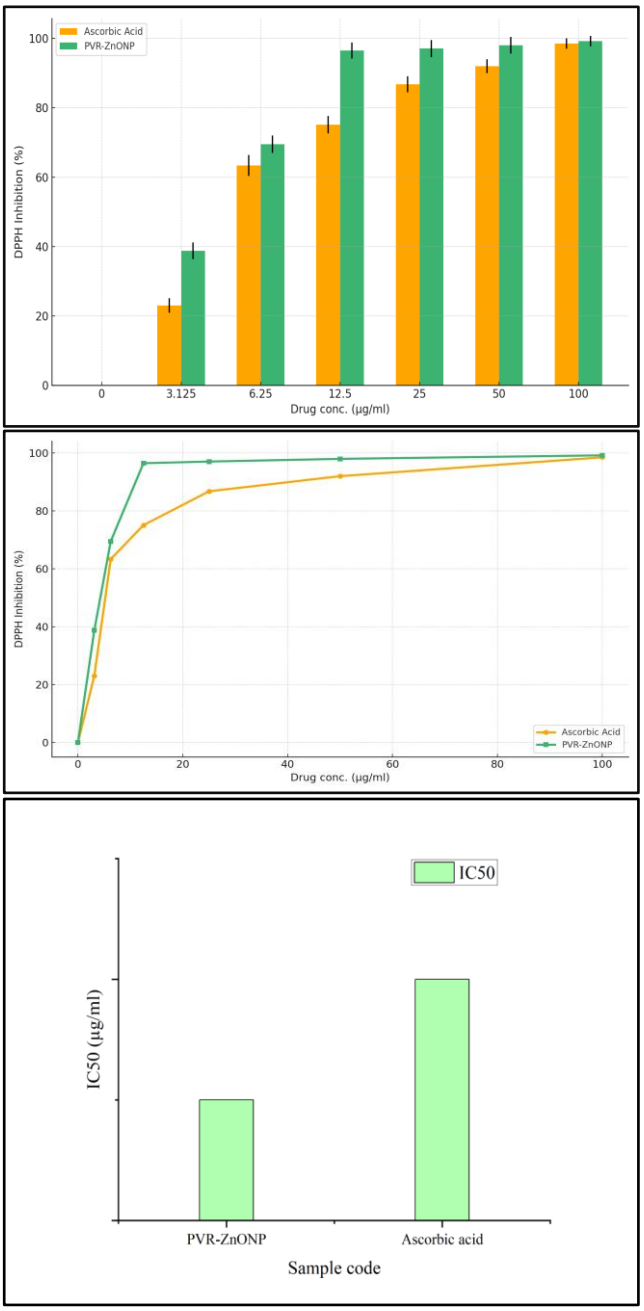

Figure 8: DPPH assay shows dose-dependent radical scavenging, with PVR ZnO nanoparticles exhibiting stronger antioxidant activity than ascorbic acid, reflected by a lower IC_{50} value (3.95 µg/mL).

ABTS Activity

The antioxidant efficacy of PVR ZnO NPs was evaluated using the ABTS [2,2′-azino-bis(3-ethylbenzothiazoline-6-sulfonic acid)] radical cation decolorization assay, with ascorbic acid serving as the standard reference. The assay demonstrated a clear concentration-dependent increase in radical scavenging activity for both PVR ZnO NPs and ascorbic acid across the tested range of 3.125 to 100 µg/mL. Notably, PVR ZnO NPs exhibited highest activity at lower concentrations, with 47.44 ± 3.0% inhibition at 3.125 µg/mL compared to 21.53 ± 2.5% for ascorbic acid. At higher concentrations, the nanoparticles consistently outperformed the standard, reaching 99.91 ± 1.5% inhibition at 100 µg/mL.

The IC_{50} value for PVR ZnO NPs was calculated as 3.65 ± 0.201 µg/mL, significantly lower than that of ascorbic acid (4.88 ± 0.250 µg/mL), indicating enhanced antioxidant potency. This elevated activity is attributed to the synergistic interaction between zinc ions and bioactive phytochemicals present in the *P. vettiveroides* root extract, which likely contribute to electron donation and stabilization of the $ABTS^{\bullet+}$ radical. These findings reinforce the potential of PVR ZnO nanoparticles as effective natural antioxidants for therapeutic and biomedical applications.

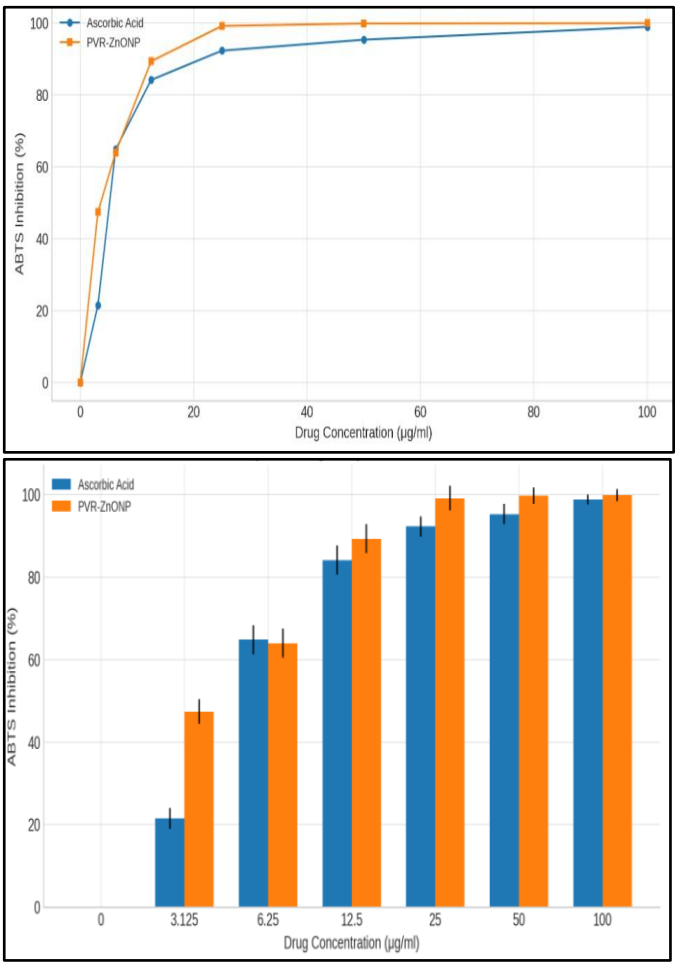

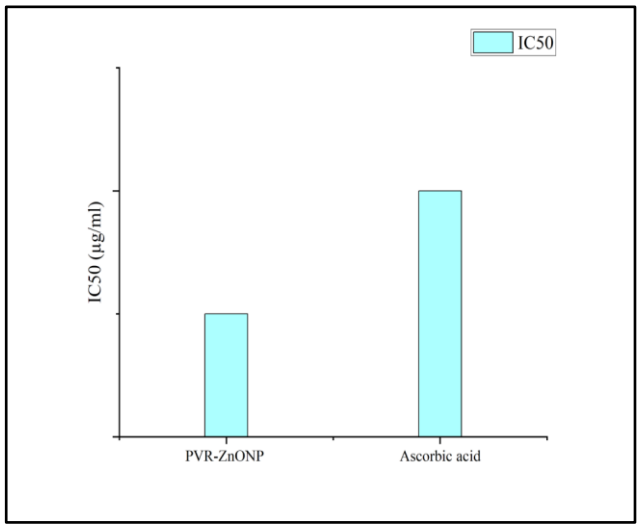

Figure 9: ABTS assay demonstrates enhanced antioxidant activity of PVR ZnO nanoparticles compared to ascorbic acid, with a lower IC_{50} value (3.65 µg/mL), indicating stronger radical scavenging efficiency.

FRAP Assay

The FRAP assay was employed to evaluate the electron-donating capacity of ZnO NPs, with ascorbic acid serving as the standard antioxidant. The assay results demonstrated a concentration-dependent increase in ferric ion reduction for both PVR ZnO NPs and ascorbic acid across the tested range of 3.125 to 100 µg/mL. At the lowest concentration (3.125 µg/mL), PVR ZnO NPs exhibited a significantly higher reducing power (45 ± 3.5 µg AAE/mL) compared to ascorbic acid (15 ± 3.0 µg AAE/mL), indicating high redox activity at low doses.

As the concentration increased, both samples showed enhanced antioxidant capacity, with PVR ZnO NPs reaching 105 ± 6.1 µg AAE/mL at 6.25 µg/mL and 158.125 ± 7.3 µg AAE/mL at 12.5 µg/mL. Although ascorbic acid demonstrated higher absolute values at higher concentrations culminating in 1071.25 ± 40.1 µg AAE/mL at 100 µg/mL the PVR ZnO NPs maintained substantial reducing activity, recording 496.25 ± 15.2 µg AAE/mL at the same concentration. These results suggest that while ascorbic acid exhibits high reducing power at higher doses, the biosynthesized ZnO nanoparticles are highly effective at lower concentrations, likely due to the synergistic interaction between zinc ions and phytochemicals from the root extract.

The consistent performance of PVR ZnO NPs across the concentration range highlights their potential as natural antioxidants with significant redox-modulating properties, suitable for therapeutic applications targeting oxidative stress.

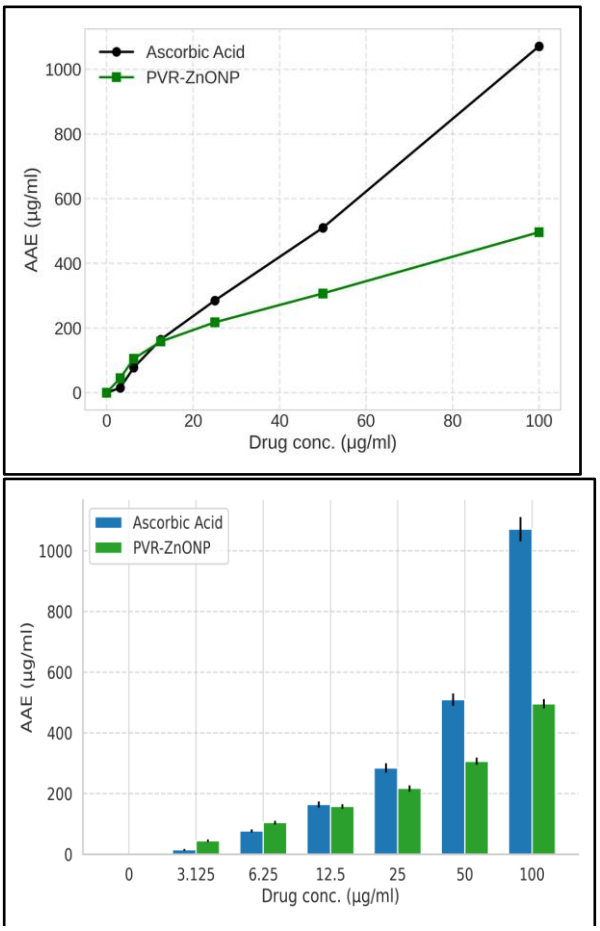

Figure 10: FRAP assay reveals dose-dependent ferric ion reduction, with PVR ZnO nanoparticles showing strong antioxidant capacity, especially at lower concentrations, compared to ascorbic acid.

Anticancer Activities of PVR ZnO NPs

MTT Cell Viability Assay

The cytotoxic potential of PVR ZnO NPs was evaluated using the MTT assay across three human cancer cell lines: A549 (lung carcinoma), HCT-116 (colorectal carcinoma), and MCF-7 (breast adenocarcinoma). Cells were treated with increasing concentrations of PVR ZnO NPs (12.5–200 µg/mL), and cell viability was assessed after 24 hours of exposure.

In A549 cells, PVR ZnO NPs exhibited a gradual reduction in viability from 97.24% at 12.5 µg/mL to 37.36% at 200 µg/mL, with an IC_{50} value of 112.07 µg/mL. Cisplatin (5 µg/mL) used as a positive control showed 44.72% viability, indicating that PVR ZnO NPs possess moderate cytotoxicity against lung carcinoma cells.

In HCT-116 cells, a more pronounced cytotoxic effect was observed, with cell viability decreasing from 91.05% at 12.5 µg/mL to 20.69% at 200 µg/mL. The IC_{50} value was calculated as 57.19 µg/mL, suggesting higher sensitivity of colorectal cancer cells to PVR ZnO NPs. Doxorubicin (1 µg/mL) reduced viability to 46.64%, confirming the comparative efficacy of the nanoparticles.

MCF-7 cells demonstrated the highest sensitivity to PVR-ZnO NPs, with cell viability dropping from 95.91% at

12.5 µg/mL to just 1.78% at 200 µg/mL. The IC_{50} value was determined to be 51.73 µg/mL, indicating potent cytotoxicity. Doxorubicin (1 µg/mL) reduced viability to 39.72%, while PVR ZnO NPs at 100 µg/mL and 200 µg/mL showed significantly greater cell death.

Overall, the MTT assay results confirm that PVR ZnO nanoparticles exhibit dose-dependent cytotoxicity, with the highest effect observed in MCF-7 cells, followed by HCT-116 and A549. These findings suggest selective anticancer potential of the biosynthesized nanoparticles, likely mediated by oxidative stress, apoptosis induction, and nanoparticle–cell membrane interactions.

Table 1: Table showed the % cell viability values of A549 cells exposed to various concentrations of PVR against the Human lung cancer (A549, HCT-116 and MCF 7) cells after the treatment period of 24hrs.

MTT Cell Viability Assay of PVR ZnO NPs of A549		
Drug conc (µg/mL)	**% cell viability**	**IC_{50} conc (ug/mL)**
Untreated	100.00	**112.07**
Cisplatin-5ug	44.72	
PVR 12.5ug	97.24	
PVR 25ug	87.36	
PVR 50ug	67.71	
PVR 100ug	51.18	
PVR 200ug	37.36	
MTT Cell Viability Assay of PVR ZnO NPs of HCT-116		
Drug conc (µg/mL)	**% cell viability**	**IC_{50} conc (ug/mL)**
Untreated	100.00	**57.19**
Dox-1ug	46.64	
PVR-12.5ug	91.05	
PVR-25ug	65.87	
PVR-50ug	53.72	
PVR-100ug	35.31	
PVR-200ug	20.69	
MTT Cell Viability Assay of PVR ZnO NPs of MCF7		
Drug conc (µg/mL)	**% cell viability**	**IC_{50} conc (ug/mL)**
Untreated	100.00	**51.73**
Dox-1ug	39.72	
PVR-12.5ug	95.91	
PVR-25ug	86.88	
PVR-50ug	50.08	
PVR-100ug	21.57	
PVR-200ug	1.78	

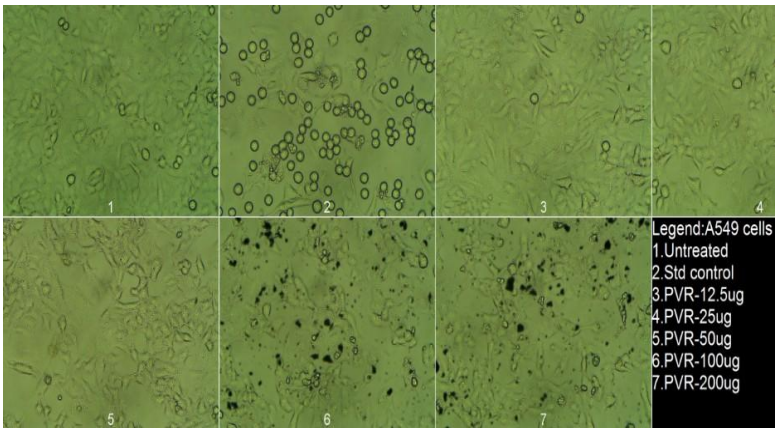

Figure 11: The morphology of A549 cells treated by different concentrations of PVR ZnO NPs after the incubation period of 24hrs. All the images were acquired under the inverted biological microscope at 20x magnification and recorded with the help of Digital camera equipped with the MICAM software.

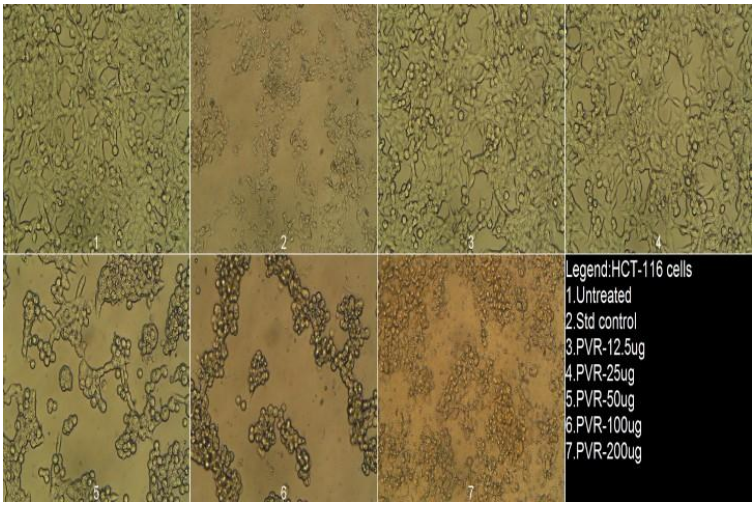

Figure 12: The morphology of HCT-116 cells treated by different concentrations of PVR ZnO NPs after the incubation period of 24hrs. All the images were acquired under the inverted biological microscope at 20x magnification and recorded with the help of Digital camera equipped with the MICAM software.

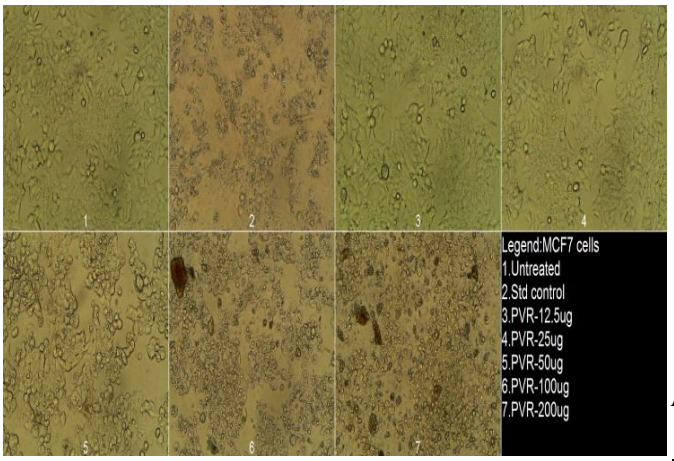

Figure 13: The morphology of MCF7 cells treated by different concentrations of PVR ZnO NPs after the incubation period of 24hrs. All the images were acquired under the inverted biological microscope at 20x magnification and recorded with the help of Digital camera equipped with the MICAM software.

Apoptosis/Necrosis Assay

The apoptotic and necrotic effects of PVR ZnO NPs were evaluated in MCF-7 cells using Annexin V-FITC/Propidium Iodide (PI) dual staining followed by flow cytometric analysis. The quadrant-based distribution revealed distinct shifts in cell populations upon treatment.

In untreated control cells, 99.68% remained viable (LL quadrant), with negligible early (0.01%) and late apoptosis (0.05%), and minimal necrosis (0.26%), confirming baseline cellular integrity. The standard control (e.g., doxorubicin or cisplatin) induced significant cell death, with 24.68% late apoptotic cells (UR), 8.59% early apoptotic cells (LR), and 4.09% necrotic cells (UL), reducing viability to 62.64%. The total apoptotic population (early + late) was 33.27%, validating the assay's sensitivity. Treatment with PVR ZnO NPs resulted in a marked increase in apoptotic cells, with 17.63% late apoptosis and 9.59% early apoptosis, totaling 27.22% apoptotic population. Necrosis was limited to 1.8%, and 70.98% of cells remained viable, indicating that the nanoparticles predominantly induce programmed cell death rather than necrotic damage.

Table 4: Table showed the % cells undergone Apoptosis, Necrosis in treated and Untreated MCF7 cells

Quadrant	%Necrotic cells	%Late apoptotic cells	%Viable cells	% Early apoptotic cells
Label	**UL**	**UR**	**LL**	**LR**
Untreated	**0.26**	**0.05**	**99.68**	**0.01**
Std control	**4.09**	**24.68**	**62.64**	**8.59**
PVR ZnO NPs	**1.8**	**17.63**	**70.98**	**9.59**

Table 5: % cells undergone Apoptosis in untreated & treated MCF7 cells by FACS.

Culture condition	% Apoptotic cells (Early+Late apoptosis)
Untreated	0.06
Std control	33.27
PVR ZnO NPs	27.22

Table 6: Meaning of the Quadrant layout in Apoptosis/necrosis study.

UL – Upper left : % of Necrotic Cells	UR - Upper right: % Late Apoptotic Cells
LL- Lower left: % Viable Cells	LR- Lower right: % of Early apoptotic cells

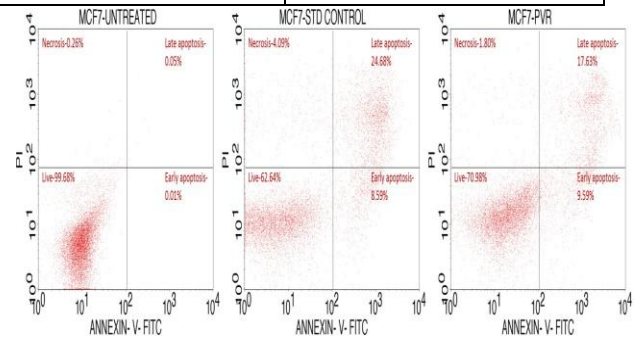

Figure 14. Quadrangular plots represented the Annexin V/PI expression in MCF7 cells in the presence and absence of PVR ZnO NPs and Std control by Flow Cytometry. Acquisition was done by using BD FACS calibar and data analyzed by BD Cell Quest Pro Software (Version: 6.0). Here, Annexin V- FITC - Primary Marker, PI- Propidium Iodide (Secondary fluorescence Marker).

Cell Cycle Study

Flow cytometric analysis of cell cycle progression in MCF-7 cells treated with of PVR ZnO NPs revealed significant alterations in DNA content distribution across key phases. In untreated control cells, the majority (81.44%) were arrested in the G_0/G_1 phase, with minimal populations in S (3.57%) and G_2/M (13.46%) phases, and only 1.53% in the sub-G_0/G_1 region, indicating healthy proliferative status and negligible apoptosis.

Upon treatment with PVR ZnO NPs, a marked shift in cell cycle dynamics was observed. The G_0/G_1 population decreased to 53.91%, while the S phase increased to 12.28%, suggesting DNA synthesis interruption and possible replication stress. The G_2/M phase also rose to 23.81%, indicating mitotic arrest. Notably, the sub-G_0/G_1 population indicative of apoptotic DNA fragmentation rose to 10%, confirming nanoparticle-induced apoptosis.

The standard control (e.g., doxorubicin or cisplatin) showed similar trends, with reduced G_0/G_1 (59.4%), elevated G_2/M (31.64%), and increased sub-G_0/G_1 (6.52%), validating the assay's sensitivity. Compared to the standard, PVR ZnO NPs induced a stronger apoptotic response and disrupted both S and G_2/M phases, suggesting a dual mechanism involving DNA damage and mitotic inhibition.

These findings demonstrate that PVR ZnO nanoparticles effectively interfere with cell cycle progression in MCF-7 cells, promoting apoptosis and cell cycle arrest, thereby reinforcing their potential as anticancer agents.

Table 7: Table showed the % cells get arrested in the different phases of MCF7 cell cycle in treated and non-treated conditions after the 24hrs of incubation.

Cell Cycle Study-MCF7 vs PVR-ZnO NPs				
Sl No	**Cell Cycle stage**	**Untreated**	**Std control**	**ZnO NPs PVR**
1	**Sub G0/G1**	**1.53**	**6.52**	**10**
2	**G0/G1**	**81.44**	**59.4**	**53.91**
3	**S**	**3.57**	**2.44**	**12.28**
4	**G2/M**	**13.46**	**31.64**	**23.81**

Figure 15: Flow cytometric histograms represented the phases of cell cycle distribution in the MCF7 cell line in Untreated as well as treated with Std and ZnO NPs PVR treatment groups after the 24hours of treatment by PI/RNase staining.

ROS Expression Study by FACS

Reactive oxygen species (ROS) generation in MCF-7 cells following treatment with of PVR ZnO NPs was quantified using DCFH-DA staining and flow cytometric analysis. The untreated control group exhibited minimal fluorescence (0.17%), indicating negligible basal ROS levels under normal culture conditions. In contrast, the standard control (e.g., doxorubicin or H_2O_2) induced a robust oxidative response, with 93.06% of cells expressing elevated DCF intensity, confirming assay sensitivity and maximal ROS induction.

Treatment with PVR ZnO NPs resulted in a significant increase in ROS positive cells, with 34.82% of the population exhibiting enhanced DCF fluorescence. This moderate yet substantial elevation suggests that the biosynthesized nanoparticles effectively induce oxidative stress, likely contributing to apoptosis and cell cycle arrest observed in complementary assays. The ROS generation is attributed to the intrinsic redox activity of ZnO and the synergistic influence of phytochemicals from the root extract, which may facilitate electron transfer and mitochondrial disruption.

These findings confirm that PVR ZnO nanoparticles trigger intracellular ROS production in cancer cells, supporting their mechanistic role in oxidative stress–mediated cytotoxicity.

Table 8: Table showed the % cells expressed ROS expression in the Untreated and treated with PVR ZnO NPs and Std conditions of MCF7 cells by FACS method.

Culture condition	**% cells expressed DCF intensity**
Untreated	0.17
Std control	93.06
ZnO NPs **PVR**	34.82

Figure 16: ROS expression study in Untreated and Treated with Std control and on the MCF7 cells by H2DCFDA staining method. % cells expressed DCF intensity in M2 region was considered for the current study.

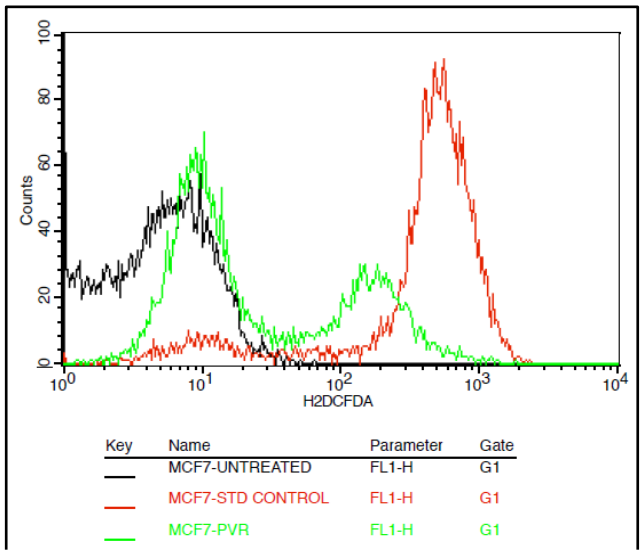

Figure 17: The DCF expression in untreated, Std control and PVR ZnO treatment on Human breast cancer (MCF7) cells. Cells without treatment were considered as control (black histogram).

Caspase-3 expression study by FACS

To elucidate the apoptotic mechanism induced by PVR ZnO NPs, intracellular Caspase-3 expression was quantified in MCF-7 cells using flow cytometry. Caspase-3, a key executioner protease in the intrinsic apoptotic pathway, serves as a reliable biomarker for programmed cell death. In untreated control cells, Caspase-3 expression was minimal (0.51%), indicating negligible basal apoptotic activity under normal culture conditions. The standard control (e.g., doxorubicin or cisplatin) induced a substantial increase in Caspase-3–positive cells (40.28%), validating the assay's sensitivity and confirming apoptosis induction via conventional chemotherapeutics.

Remarkably, treatment with PVR ZnO NPs resulted in a pronounced elevation of Caspase-3 expression, with 65.82% of cells exhibiting high fluorescence intensity. This significant upregulation suggests that the biosynthesized nanoparticles effectively activate the intrinsic apoptotic cascade, likely through mitochondrial disruption and oxidative stress, as supported by complementary ROS and Annexin V/PI data.

These findings confirm that PVR ZnO nanoparticles not only induce apoptosis but do so via Caspase-3–dependent pathways, reinforcing their potential as targeted anticancer agents with mechanistic specificity.

Table 9: Table showed the % cells expressed Caspase-3 expression in the Untreated and treated with ZnO NPs PVR and Std conditions of A549 cells by Flow Cytometry.

Culture condition	% cells expressed Caspase-3 intensity
Untreated	0.51
Std control	40.28
PVR ZnO NPs	65.82

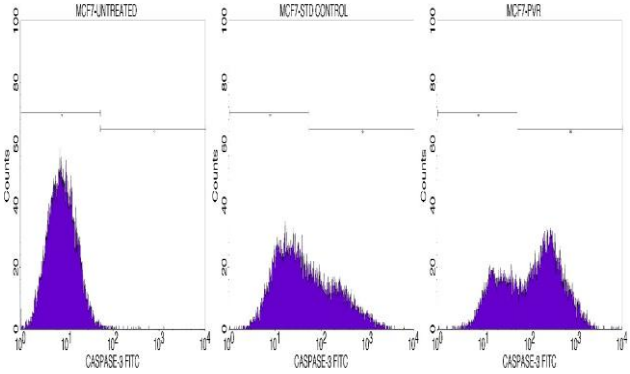

Figure 18: Caspase-3 expression study in untreated and Treated with Std control and PVR ZnO NPs on the MCF7 cells after 24hours of incubation. % cells expressed Caspase-3 intensity in M2 region was considered for the current study.

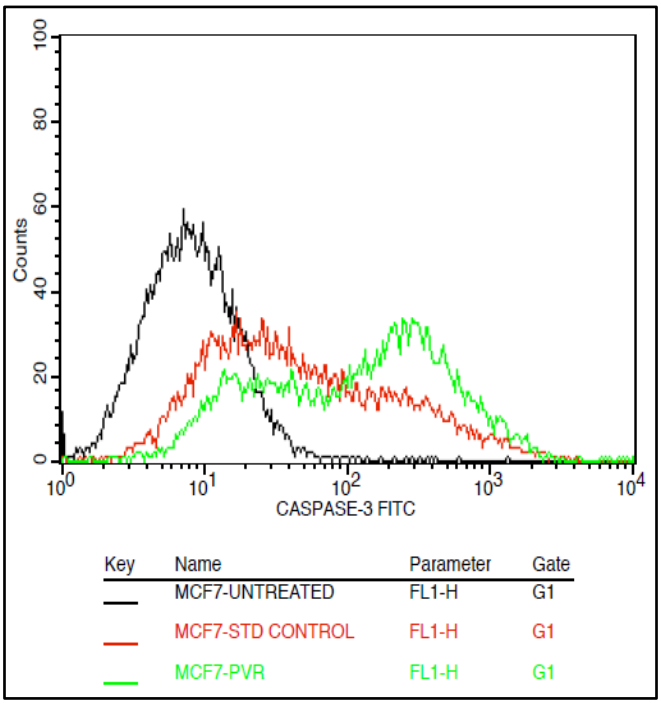

Figure 19: The Caspase-3 expression in untreated, Std control and PVR ZnO NPs treatment on Human breast cancer (MCF7) cells. Cells without treatment were considered as control (black histogram).

DISCUSSION

The present study demonstrates the successful green synthesis of ZnO NPs using *P. vettiveroides* root extract, and evaluates their physicochemical properties, antioxidant potential, photocatalytic activity, and anticancer efficacy across multiple human cancer cell lines. The UV-Vis spectral analysis revealed a characteristic absorption peak at 275 nm for the root extract and a blue shift in ZnO NPs absorption, indicating reduced particle size and successful nanoparticles formation. FTIR analysis confirmed the presence of functional groups such as hydroxyl, alkene, and halogen stretches, along with Zn–O vibrations, suggesting phytochemical-mediated reduction and stabilization of ZnO NPs. These findings align with previous reports where plant-derived biomolecules facilitated nanoparticle synthesis through hydroxyl and carboxyl interactions (Iravani *et al*., 2014).

Morphological characterization via SEM and HR TEM revealed irregular, aggregated nanostructures with porous surfaces and grainy texture, typical of biosynthesized metal oxides. HR TEM at higher magnifications showed sintered particles with low crystallinity and uneven contrast. EDAX analysis validated the elemental composition, with Zn and O being predominant, confirming the purity of ZnO NPs. Particle size analysis indicated a D_{50} of 92.6 nm, and zeta potential of −25.6 mV, suggesting moderate colloidal stability and negative surface polarity, consistent with reports by Ramesh *et al*. (2016) on plant mediated ZnO NPs.

The antioxidant potential of PVR ZnO NPs was evaluated using DPPH, ABTS, and FRAP assays. In all three assays, the nanoparticles exhibited dose-dependent radical scavenging activity, outperforming ascorbic acid at lower concentrations. The IC_{50} values for DPPH (3.95 µg/mL) and ABTS (3.65 µg/mL) were significantly lower than the standard, indicating potent antioxidant capacity. FRAP assay further confirmed strong ferric ion reducing power, especially at low doses. These results are in agreement with studies by Zaza *et al*. (2022), who reported enhanced antioxidant activity of NPs synthesized using *Ocimum sanctum*.

Photocatalytic degradation of methylene blue dye under UV light revealed a time-dependent increase in degradation efficiency, reaching 59.56% at 180 minutes. The porous morphology and moderate particle size likely contributed to enhanced surface area and light absorption, facilitating ROS generation and dye breakdown. Similar photocatalytic behavior has been reported for biosynthesized ZnO NPs by Singh *et al*. (2026), reinforcing their environmental applicability.

The anticancer potential of PVR ZnO NPs was assessed via MTT assay across A549, HCT-116, and MCF-7 cell lines. The nanoparticles exhibited dose-dependent cytotoxicity, with IC_{50} values of 112.07 µg/mL (A549), 57.19 µg/mL (HCT-116), and 51.73 µg/mL (MCF-7), indicating selective efficacy. Notably, MCF-7 cells showed the highest sensitivity, suggesting potential for breast cancer therapy. These findings are supported by earlier studies where ZnO NPs induced cytotoxicity via oxidative stress and apoptosis (Premanathan *et al*., 2011).

Flow cytometry–based Annexin V/PI staining revealed a significant increase in apoptotic cells (27.22%) upon PVR-ZnO NPs treatment, with minimal necrosis, indicating activation of programmed cell death. Cell cycle analysis showed arrest at S and G_2/M phases, along with an increase in sub-G_0/G_1 population, confirming DNA fragmentation and mitotic inhibition. ROS expression analysis demonstrated a 34.82% increase in DCF-positive cells, suggesting oxidative stress as a key mechanism. Caspase-3 expression was markedly elevated (65.82%), validating the activation of intrinsic apoptotic pathways. These mechanistic insights are consistent with the work of Sahu *et al.* (2017), who reported ZnO NPs induced apoptosis via ROS-mediated mitochondrial disruption and caspase activation.

Collectively, the study establishes that PVR ZnO nanoparticles synthesized via a green route possess multifunctional properties antioxidant, photocatalytic, and anticancer driven by their unique phytochemical composition and nanoscale architecture. The integration of traditional medicinal plant extracts with nanotechnology offers a sustainable and biocompatible platform for therapeutic and environmental applications. The findings not only reinforce the biomedical relevance of ZnO NPs but also highlight the translational potential of *Plectranthus vettiveroides* as a novel bioresource in nanomedicine.

CONCLUSION

This study successfully demonstrates the green synthesis of ZnO NPs using *P. vettiveroides* root extract, yielding biocompatible nanostructures with multifunctional properties. The phytochemical constituents of the extract played a pivotal role in reducing, stabilizing, and capping the nanoparticles, as confirmed by UV-Vis, XRD, FTIR, SEM, HR TEM, EDAX, and zeta potential analysis. The biosynthesized PVR ZnO NPs exhibited potent antioxidant activity, outperforming standard ascorbic acid in DPPH, ABTS, and FRAP assays, and showed promising photocatalytic degradation of methylene blue dye, highlighting their environmental relevance.

Biological evaluations revealed selective cytotoxicity against A549, HCT-116, and MCF-7 cancer cell lines, with MCF-7 showing the highest sensitivity. Flow cytometry studies confirmed that PVR ZnO NPs induce apoptosis via ROS generation, caspase-3 activation, and cell cycle arrest at S and G_2/M phases, with minimal necrotic damage. These mechanistic insights affirm the therapeutic potential of PVR ZnO NPs as targeted anticancer agents.

Overall, the integration of traditional medicinal plant resources with nanotechnology offers a sustainable and effective platform for biomedical and environmental applications. The findings underscore the translational value of *Plectranthus vettiveroides* mediated ZnO nanoparticles and pave the way for future investigations into their clinical and ecological utility.

REFERENCES

1. Sukri , S. N. A., Shameli, K., Teow, S.-Y., Chew, J., Ooi, L.-T., Lee-Kiun Soon, M., Ismail, N. A., & Moeini, H. (2023). Enhanced antibacterial and anticancer activities of plant extract mediated green synthesized zinc oxide-silver nanoparticles. Frontiers in Microbiology, 14, Article 1194292. https://doi.org/10.3389/fmicb.2023.1194292.

2. Golzarnezhad, F., Allahdou, M., Mehravaran, L. et al. (2025).Green synthesis of ZnO nanoparticles from the extract of *Cymbopogon olivieri* and investigation of their antimicrobial and anticancer effects. Discov Appl Sci 7, 196. https://doi.org/10.1007/s42452-025-06623-z

3. Fatima, K., Asif, M., Farooq, U., Gilani, S. J., Bin Jumah, M. N., & Ahmed, M. M. (2024). Antioxidant and anti-inflammatory applications of *Aerva persica* aqueous-root extract-mediated synthesis of ZnO nanoparticles. ACS Omega, 9(14), 15882–15892.

4. Momeni,A., Meshkatalsadat M.H., & Pouramiri. B. (2023).Catalytic, Antioxidant, and Antifungal Applications of ZnO Nanoparticles. Facile Green Synthesis by *Crataegus oxyacantha* Leaf Aqueous Extract. BioNanoSci,14, 457–473. https://doi.org/10.1007/s12668-023-01238-3.

5. Perumal, P., Sathakkathulla, N. A., Kumaran, K., Ravikumar, R., Selvaraj, J. J., Nagendran, V., Gurusamy, M., Shaik, N., Prabhakaran, S. G., Palanichamy, V. S., Ganesan, V., Thiraviam, P. P., Gunalan, S., & Rathinasamy, S. (2024). Green synthesis of zinc oxide nanoparticles using aqueous extract of shilajit and their anticancer1. activity against HeLa cells. Scientific Reports, 14, Article 2204. https://doi.org/10.1038/s41598-024-52217-x.

6. Premanathan M., Karthikeyan K., Jeyasubramanian K., Manivannan G .(2011). Selective toxicity of ZnO nanoparticles toward Gram-positive bacteria and cancer cells by apoptosis through lipid peroxidation. Nanomedicine,7(2),18492.doi:10.1016/j.nano.2010.10.01.

7. Chandrasekar, L. P., Sethuraman, B. D., Subramani, M., & Mohandos, S. (2023). Green synthesised ZnO nanoparticles from *Plectranthus amboinicus* plant extract: Removal of Safranin-O and Malachite green dyes & anti-bacterial activity. International Journal of Environmental Analytical Chemistry, 104.

8. Pandey OP, Kaur J, Sharma M. (2013). Effect of pH on photocatalytic activity of capped ZnS nanoparticles. J Nanosci Nanotechnol, Jul;13(7): 4861-71. doi: 10.1166/jnn.2013.7598.

9. Ala-Nissila., Aki Kutvonen., Giulia Rossi., Sakari R., Puisto., Niko K. J. Rostedt, Tapio. (2012). Influence of nanoparticle size, loading, and shape on the mechanical properties of polymer nanocomposites. *J. Chem. Phys.* 7; 137 (21), 214901.

10. Shah, Pooja., & Modi, H. (2015). Comparative Study of DPPH, ABTS and FRAP Assays for Determination of Antioxidant Activity.International journal for research in applied science and Engineering Technology, vol.3, Article : 2321-9653.

11. Iravani, S., Korbekandi, H., Mirmohammadi, S. V., & Zolfaghari, B. (2014). Synthesis of silver nanoparticles: Chemical, physical and biological methods. Research in Pharmaceutical Sciences, 9(6), 385–406.

12. Chaves N., Santiago A., Alías JC. (2020). Quantification of the Antioxidant Activity of Plant Extracts: Analysis of Sensitivity and Hierarchization Based on the Method Used. Antioxidants (Basel), 15,9(1),76. doi: 10.3390/antiox9010076. PMID: 31952329; PMCID: PMC7023273.

13. Singh, D., Khan, F., Jain, V.K. *et al.* (2026). Enhanced Photocatalytic Activity of Sol–Gel Derived Ruthenium-Doped Titanium Dioxide (Ru@TiO_2) Photocatalyst for the Degradation of Two Hazardous Dyes. *Water Air Soil Pollut*, 237, 477.https://doi.org/10.1007/s11270-026-09091-2.

14. Asif, M., Shafiq, M., Imtiaz, F. *et al.* (2025). Photocatalytic Degradation of Methyl Orange from Aqueous Solution Using ZnO by Response Surface Methodology. *Top Catal* 68, 814–822. https://doi.org/10.1007/s11244-024-01969-x.

15. Sahu N., Meena S., Shukla V., Chaturvedi P., Kumar B., Datta D., Arya KR. (2017). Extraction, fractionation and re-fractionation of Artemisia nilagirica for anticancer activity and HPLC-ESI-QTOF-MS/MS determination. Journal of Ethnopharmacology, Volume 213 ,Pages 72-80,ISSN 0378-8741. https://doi.org/10.1016/j.jep.2017.10.029.

16. Ramesh, N., Rao, M.G., Varala, R. *et al.* (2016). Mercuric chloride catalyzed synthesis of some anticancer 2-aryl-2,3-dihydroquinizolin-4(1*H*)-ones. (2016).*Med Chem Res* 25, 1945–1951.https://doi.org/10.1007/s00044-016-1630-y.

17. Fox R.,Aubert M.(2008).Flow cytometric detection of activated caspase-3. Methods Mol Biol. 2008;414:47-56. doi: 10.1007/978-1-59745-339-4_5. PMID: 18175811.

18. Srivatsa A., Adiga D., Chopra A., Lobo R, Kabekkodu SP, Gadag S., Nayak U., Sivaraman K., Shah A. (2022) Goji berry (Lycium barbarum) inhibits the proliferation, adhesion, and migration of oral cancer cells by inhibiting the ERK, AKT, and CyclinD cell signaling pathways: an in-vitrostudy.F1000Res.22;11:1563.doi:10.12688/f1000research.129250.3. PMID: 36761830; PMCID: PMC9887205.

19. Rajkumar V., Guha, Gunjan, & Kumar, R. & Mathew, Lazar. (2017). Evaluation of Antioxidant Activities of Bergenia ciliata Rhizome. Records of Natural Products. 4. 38-48.

19. Zaza Melkamu., P R Jeyaramraja ., Taddesse Paulos. (2022). Optimization of the synthesis of silver nanoparticles using the leaf extract of *Ocimum sanctum* and evaluation of their antioxidant. potential.Nano Express, Volume 3, Number 3. DOI 10.1088/2632-959X/ac8fac